Available online at www.sciencedirect.com
SCIENCE DIRECT®
Nuclear Instruments and Methods in Physics Research A 505 (2003) 531–535
NUCLEAR INSTRUMENTS & METHODS IN PHYSICS RESEARCH Section A
www.elsevier.com/locate/nima

Two aspects of thin film analysis: boron profile and scattering length density profile

H.H. Chen-Mayer[a,*], G.P. Lamaze[a], K.J. Coakley[b], S.K. Satija[c]

[a] *Analytical Chemistry Division, National Institute of Standards and Technology, Gaithersburg, MD 20899, USA*
[b] *Statistical Engineering Division, National Institute of Standards and Technology, Boulder, CO 80305, USA*
[c] *Center for Neutron Research, National Institute of Standards and Technology, Gaithersburg, MD 20899, USA*

Abstract

Boron/phosphorus-doped silicate glass (BPSG) thin films are widely used in microelectronic circuit devices. We employ two neutron techniques to investigate a 200-nm thick BPSG film: neutron depth profiling (NDP) and neutron reflectometry (NR) to obtain complementary information on the boron containing layer.

PACS: 61.12.Ha; 29.30.Ep; 68.55.Ln

Keywords: Neutron depth profiling; Boron distribution; Neutron reflectivity

1. Introduction

Neutron depth profiling (NDP) is a technique based on neutron capture by certain isotopes such as ^{10}B, ^{6}Li, and ^{14}N, and the subsequent emission of charged particles [1]. The energy and intensity of these particles contain information about the concentration *and* depth distribution of the light element. Microelectronic circuit devices widely employs boron/phosphorus-doped silicate glass (BPSG) thin films that require careful control of the boron concentration in the manufacturing processes. Using the products from the nuclear reaction ^{10}B(n,α)^{7}Li, NDP can determine the total boron concentration in the film by direct comparison to a matrix-independent calibration standard. Therefore, NDP can serve as a concentration calibration of many of the on-line and off-line measurement techniques such as secondary ion mass spectrometry (SIMS) [2]. This paper emphasizes the boron spatial distribution profile derived from an NDP measurement, and predicts the boron profile from a density profile obtained from a neutron reflectivity measurement. In reflectometry, one measures the angular dependence of the specular reflectivity near grazing incidence. By fitting models based on some prior knowledge to the reflectivity data, parameters representing features such as film thickness, density, and interface roughness can be determined [3]. While NDP measures only the boron isotope in the matrix, reflectometry measures the total scattering contribution from the matrix and is not sensitive

*Corresponding author. Tel.: +1-301-975-5595; fax: +1-301-208-7682. Current affiliation: Ionizing Radiation Division, NIST, Gaithersburg, MD 20899, USA.
E-mail address: chen-mayer@nist.gov (H.H. Chen-Mayer).

0168-9002/03/$ - see front matter
doi:10.1016/S0168-9002(03)01139-2

to the low level of boron. Because NR and NDP are based on entirely different principles, the information obtained is independent and can be used to verify or modify NDP results in film thickness represented by the boron profile. We have previously presented a comparison study based on BPSG samples using NDP and NR techniques [4] without taking into account the various effects that broaden the NDP spectrum. New reflectivity data have now been obtained over a greater angular range with an improved signal-to-noise ratio, yielding a more reliable density profile. We report additional NDP analysis examining the various broadening factors, and predict the observed NDP spectrum based on the density profile model obtained from the new NR data.

2. Measurements and data analyses

The sample is a 150-mm-diameter silicon wafer of about 0.25 mm thickness, with a CVD (chemical vapor deposition) BPSG film (2 wt.% boron) nominally 200 nm thick, and with a 20 nm thick silicon dioxide surface coating. Both NDP and NR measurements have been performed at the NIST Center for Neutron Research (NCNR). The NDP facility [5] is located at the end of a short curved guide (NG0) viewing the cold source. For the NDP measurement, the $1\,\sigma$ uncertainty due to the counting statistics is about 2% per channel at best. The neutron reflectivity (NR) data has been collected at the reflectometry spectrometer at NG7 (neutron wavelength 0.476 nm). The reflectivity recorded as a function of the grazing incident angle spans 5 orders of magnitude. The $1\,\sigma$ uncertainty due to the counting statistics per angular step (step size $5\times10^{-4}\,\text{Å}^{-1}$) is from 2.5% to 10%. The data and the least-squared fit using the NIST software MLAYER are shown in Fig. 1. The model used for the fit accounts for layer thickness, roughness, and the scattering length density (SLD, proportional to the density). The model that yields the best fit is also shown in Fig. 1. The BPSG density of $2.362\,\text{g/cm}^3$, derived from the SLD, is used in obtaining the NDP spatial profile.

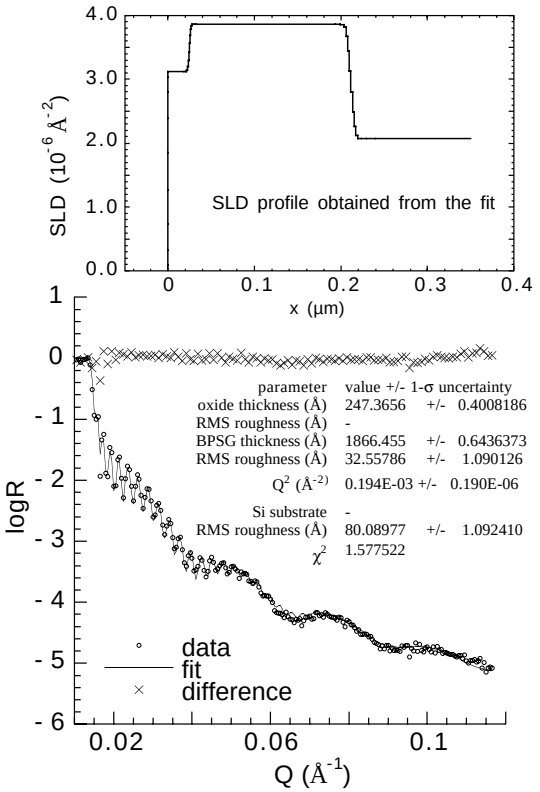

Fig. 1. Main plot: Neutron reflectivity (on log scale) obtained from a thin film sample of BPSG on silicon, and the minimum chi-squared fit to the data based on a model consisting of SiO_2/BPSG/Si substrate (see top inset). The difference between the fit and data is also plotted. The high frequency oscillations are from the thicker BPSG layer, whereas the lower frequency ones manifested at higher Q are due to the thinner surface oxide layer. Top insert: SLD profile obtained from the fit—the step shown near the surface represents the surface oxide layer.

In NDP, the residual energy spectrum, $N(E)$, of the charged particles created by the boron capture reaction within the BPSG film, is recorded as counts within each energy bin by a surface barrier detector located 71° from the normal of the sample with an energy bin width of 0.8 keV/channel on the multichannel analyzer. A thin boron metal surface deposit is used for energy calibration. $N(E)$ is a convolution of the true boron distribution, $C(x)$, with a detector response function $F(E,x)$ [6]:

$$N(E)=\int_0^R \mathrm{d}x\, C(x)\, F(E,x) \tag{1}$$

where $F(E,x)$ correlates the energy response to a charged particle coming from depth x. For a given x, $F(E,x)$ is the expected normalized energy spectrum that would be determined. The shape of $F(E,x)$ depends on four main contributing factors: the energy resolution of the detector, straggling, multiple scattering, and geometry. $E(x)$ is the measured residual energy of the charged particle after traversing a distance x in the matrix, given by

$$x = \int_{E_0}^{E(x)} \mathrm{d}E/S(E) \qquad (2)$$

where $S(E) = -\mathrm{d}E/\mathrm{d}x$ is the stopping power, or energy loss per unit thickness, of the charge particle in the matrix which can be calculated [7].

Without knowledge of $F(E,x)$, a direct conversion of $N(E)$ to $N(x)$ can be done using Eq. (2), as treated in the earlier work [4]. However, the true distribution $C(x)$ can only be obtained by deconvolution of Eq. (1). Fig. 2 shows $N(x)$ as compared with the SLD profile obtained from NR, indicating a much broader distribution obtained by NDP than the SLD profile from NR. We now evaluate the four contributions to the broadening of the NDP spectrum. For convenience, we compute a standard deviation σ_E associated with each contributing source of energy broadening. The detector energy resolution is spatially invariant and is estimated from a measurement of the energy spectrum from a surface deposit. The geometric factor is determined by calculating a distribution of the trajectories along the direction cosine. The straggling and multiple scattering factors are obtained following the models used in Refs. [6, 8]. The contributions from these physical effects are plotted in Fig. 3 as a function of depth. The values at the midpoint of the trailing edge in Fig. 2 are tabulated in Table 1. The width of the edges of $N(x)$ in Fig. 2 can be estimated by the derivative $\mathrm{d}N/\mathrm{d}x$, which approximately follows a Gaussian distribution with a variance σ^2_{data}. The values of σ_{data} for the leading and the trailing edges are, respectively, 9.6 ($\pm$2.1) and 21.9 ($\pm$7.2) keV. The latter is essentially the same as the total σ_E in Table 1, whereas the former is dominated by the detector energy resolution. Therefore, the NDP data do not suggest any measurable boron

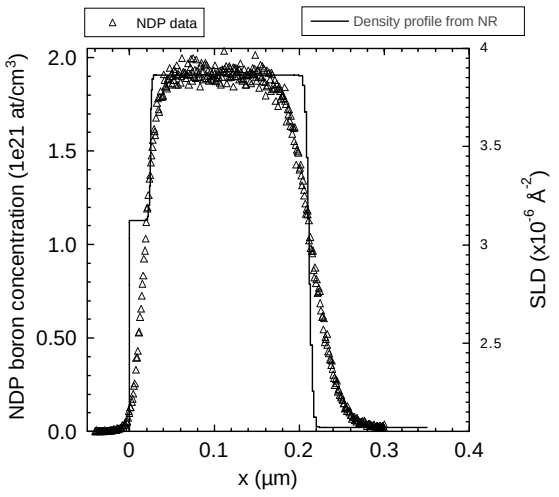

Fig. 2. Boron depth profile, proportional to $N(x)$, obtained directly from NDP, compared with the SLD profile from NR.

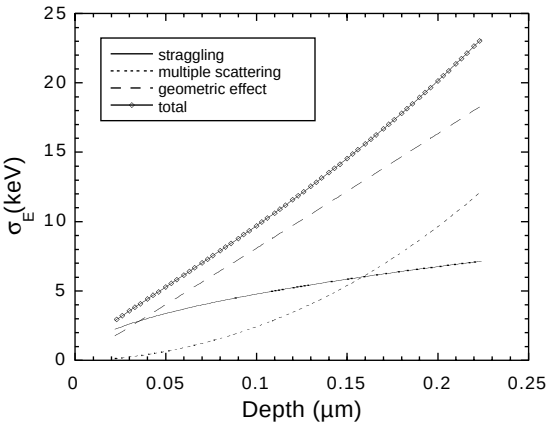

Fig. 3. Energy broadening $\sigma_{E(x)}$ due to straggling, multiple scattering, and geometric effect as a function of depth.

Table 1
Calculated contributions to the broadening of the boron distribution profile for the trailing edge at 1285 keV (Fig. 3 at 0.212 μm)

Contribution	Method used	σ_E (keV)	$\Delta\sigma_E$ (keV)
Det. res.	Measurement	8.69	0.027
Straggling	Model calc. [6]	6.93	—
Mult. scatt.	Model calc. [6]	10.80	—
Geometry	Simulation	17.35	0.87
Total	Quadrature sum	23.26	0.87

$\Delta\sigma_E$ is the estimated 1 standard deviation of σ_E.

diffusion into either the oxide layer or the silicon substrate.

3. Model prediction of NDP spectrum

We take a step further to simulate the NDP spectrum based on the measured spatial profile from NR. To obtain an expected value $<N(E_k)>$ of the observed value $N(E_k)$ (counts at energy E_k), the integral in Eq. (1) has been expressed in a vector form with the response function $F(E,x)$ in a form of a probability transition matrix [8]:

$$\langle N(E_k)\rangle = \sum_j F(k,j)\, C(xj), \tag{3}$$

where k denotes the energy observation bin and j the depth increment. For a particular depth x_j, $F(k,j)$ is obtained by a numerical integration method. We first compute the distribution of direction cosines for detected particles. For each depth, we compute the distribution of path lengths. For each path length value, we compute the expected energy $E(x_j)$ of the particle after it exits the sample. We translate the energy resolution function of the detector so that it is centered at this expected energy. We convolve the translated energy resolution function with a Gaussian which has a standard deviation equal to the overall RMS broadening due to straggling and multiple scattering. We then take a weighted average of the expected energy spectra for all the possible trajectories. The weights are determined from solid angle factors. The jth column represents the expected energy spectrum corresponding to a delta function signal originated at the jth depth x_j. This is illustrated in Fig. 4, where six sample columns of $F(k,j)$ are shown, representing the increasing broadening at greater depths.

Assuming that the true boron distribution $C(x)$ follows the measured BPSG SLD profile from NR, an NDP spectrum $<N(E)>$ can be predicted using Eq. (3) with the same bin width as the experimental one. The expected residual energy $E(x)$ is calculated with a stopping power (using TRIM [7] but corrected for the 5% error [8] for the fraction of Si) in the BPSG matrix and is subsequently corrected for the additional SiO_2 over layer. This prediction is compared to the

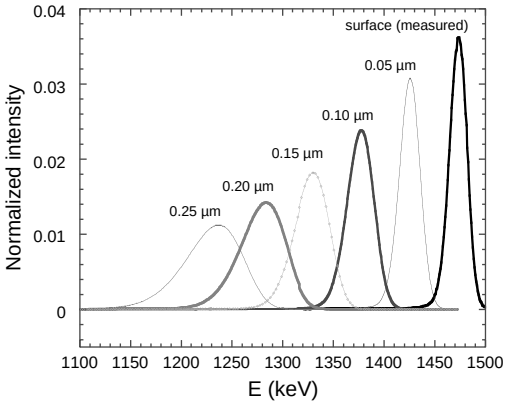

Fig. 4. The six selected columns from the detector response function matrix, representing the expected energy distribution at various depths. The surface distribution is a measured spectrum from a thin boron deposition used as energy calibration.

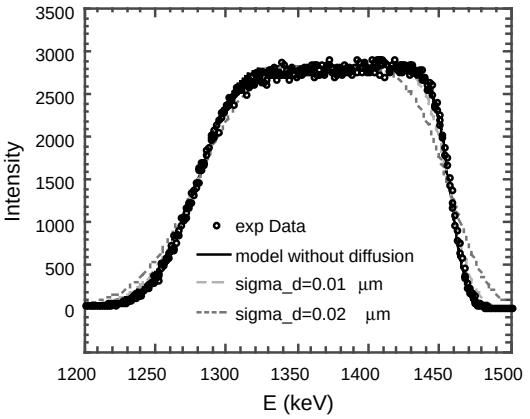

Fig. 5. Comparison of a simulated NDP energy spectrum to the experimental data (no diffusion). The stopping power in the BPSG matrix has been corrected for the SiO_2 over layer. Modeling of diffusion with a width of 0.01 and 0.02 μm are also shown.

experimental energy spectrum in Fig. 5. The excellent agreement found between the model prediction and the measured NDP spectrum shows that the model obtained from NR describing the BPSG profile can also be used to describe the boron distribution, again verifying that there is little diffusion of boron into the adjacent layers. Simulated diffusion with a given width (σ_d) shows the broadening that would be observed. This study provides a basis for future NDP spectrum

deconvolution for systems with a near-step function distribution.

Acknowledgements

We thank Julie Borchers and Rob Ivkov for help in the NR data analysis and David Mildner for discussions.

References

[1] R.G. Downing, G.P. Lamaze, in: W.M. Bullis, D.G. Seiler, A.D. Diebold (Eds.), Semiconductor Characterization: Present Status and Future Needs, AIP Press, Woodbury, NY, 1996, pp. 346–350.

[2] D.S. Simons, P.H. Chi, R.G. Downing, G.P. Lamaze, in: W.M. Bullis, D.G. Seiler, A.D. Diebold (Eds.), Semiconductor Characterization: Present Status and Future Needs, AIP Press, Woodbury, NY, 1996, p. 382.

[3] J.A. Dura, C.F. Majkrzak, in: W.M. Bullis, D.G. Seiler, A.D. Diebold (Eds.), Semiconductor Characterization: Present Status and Future Needs, AIP Press, Woodbury, NY, 1996, pp. 549–554.

[4] H.H. Chen-Mayer, G.P. Lamaze, S.K. Satija, Proceedings of the 2000 International Conference on Characterization and Metrology for ULSI Technology, Gaithersburg, Maryland, June 2000, in: D.G. Seiler, et al., (Eds.), AIP Conference Proceedings 550, Melville, New York, 1999, pp. 407–411.

[5] G.P. Lamaze, H.H. Chen-Mayer, J.K. Langland, Characterization and Metrology for ULSI Technology: 1998 International Conference, in: D.G. Seiler, W.M. Bullis, T.J. Shaffner, R. McDonald, E.J. Walters (Eds.), AIP Conference Proceedings 449, Woodbury, New York, 1998, pp. 883–886.

[6] J.T. Maki, R.M. Fleming, D.H. Vincent, Nucl. Instr. and Meth. B 17 (1986) 147.

[7] J.F. Ziegler, Public domain computer code, SRIM-2000, IBM-Research/Yorktown, New York, 10598, USA.

[8] K.J. Coakley, H.H. Chen-Mayer, G.P. Lamaze, D.S. Simons, P.E. Thompson, Nucl. Instr. and Meth. B 192 (2002) 349.